

Rapid Production of Submicron Drug Substance Particles by Supersonic Spray Drying

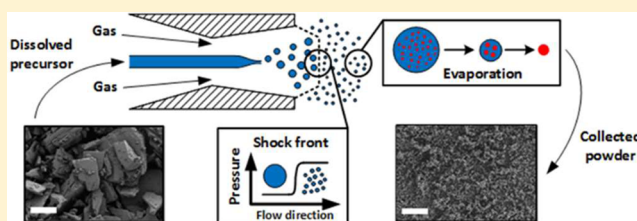
Maximilian L. Eggersdorfer,^{†,‡,||} Vitaly Koren,^{†,‡,⊥} Elad Stolovicki,[†] Esther Amstad,[‡] and David A. Weitz^{*,†,§,Ⓢ}

[†]School of Engineering and Applied Sciences and [§]Department of Physics, Harvard University, Cambridge, Massachusetts, United States

[‡]Institute of Materials, Ecole Polytechnique Fédérale de Lausanne, Lausanne, Switzerland

S Supporting Information

ABSTRACT: Many newly developed active pharmaceutical ingredients (APIs) are poorly soluble in water and thus have a dissolution-limited bioavailability. The bioavailability of Biopharmaceutical Classification System (BCS) class II APIs increases if they dissolve faster; this can be achieved by increasing their surface-to-volume ratio, for example, through formulation as submicron particles. In this paper, we develop a supersonic spray dryer that enables rapid synthesis of submicron-sized APIs at room temperature. Dispersing gas is



accelerated to supersonic velocities in the divergent portion of a de Laval nozzle. The API solution is directly injected in the divergent portion and fully nebulized by impinging high velocity gas and pressure gradients across shocks at the exit of the nozzle. In such a device, we produce crystalline danazol particles with a Sauter mean diameter as small as 188 nm at a production rate up to 200 mg/h. The smallest particles with the narrowest size distributions are formed in overexpanded flows with a shock front close to the nozzle exit. Moreover, we demonstrate the scalability up to 1500 mg/h by increasing the danazol solution concentration; in this case, the Sauter mean diameter of the spray-dried particles increases to 772 nm.

INTRODUCTION

Active pharmaceutical ingredients (APIs) are constituents of a drug that are absorbed by the body and cause a dose-dependent effect.¹ The absorption rate of APIs and thus their bioavailability are directly related to their dissolution kinetics in water so they can be delivered in the body.^{2,3} Unfortunately, approximately 70% of newly developed API candidates² and 40% of marketed drug substances³ show poor dissolution kinetics in water.⁴ The dissolution kinetics of a drug substance can be increased by chemical^{5,6} or physical structure modifications. Chemical modifications can be used to make the molecules more hydrophilic through, for example, salt formation of ionizable APIs⁶ or complexation,^{7,8} or the dissolution can be improved through the use of surfactants and cosolvents.⁹ However, such modifications must be developed for each drug individually making them cost and labor intensive;¹⁰ in addition, they may introduce impurities and, in some cases, decrease the drug efficacy.^{9,11,12} An alternate method to increase drug substance bioavailability is through physical modification by formulating it as very small particles since the dissolution rate scales with the surface-to-volume ratio.¹³ A reduction in the particle size leads to an increase in specific surface area¹⁴ and thereby increases the dissolution rate.¹⁵ Common approaches to reduce the particle size include top-down techniques such as milling¹⁶ as well as bottom-up routes such as nanoprecipitation and spray drying.^{17,18} Milling is a power-consuming process¹⁹ that can alter the particle's crystal

structure, form polymorphs, and result in polydisperse particles with poorly defined dissolution kinetics.²⁰ Nanoprecipitation is a one-step synthesis process which produces nanoparticles with a narrow size distribution.²¹ However, this technique is challenging to scale-up as it requires precise control of reactor conditions to achieve the desired product properties; small changes in process conditions can compromise batch-to-batch reproducibility.¹⁹ By contrast, spray drying enables continuous and scalable production of API particles.⁵ In this process, a carrier gas is used to form drops of a solution of API molecules. As the solvent evaporates, the droplets shrink and the solute concentration in the drop continuously increases. Once the solute concentration exceeds the saturation concentration, particles of the drug begin to nucleate. The nuclei grow as the solvent is evaporated forming a solid particle of the drug. The size of the drug particle produced is determined by the droplet size; improved bioavailability requires at least sub-micrometer sized drug particles, and these in turn require small drops to be formed in the spray dryer. The size of the droplets produced is determined by the minimal feature size of the spray-dryer nozzle as well as the shear rate and surface tension between solvent and dispersing gas.²² To produce sub-micrometer size drug particles typically requires droplets below a few microns in

Received: January 8, 2017

Revised: March 3, 2017

Published: March 3, 2017

diameter, and this limits the production rate of the drops and hence the throughput of the spray dryers. For example, the throughput of a commercial spray dryer that produces sub-micrometer particles is limited to production rates of mg/h.^{23,24} However, early phase development studies of drug particles require approximately 50 g.²⁵ Thus, a spray dryer that is capable of significantly higher production rates would be of considerable value for these applications. Unfortunately, such a spray dryer does not exist. Such a device would significantly reduce the processing time and greatly facilitate the formulation of poorly water-soluble drug substances into submicron particles.

In this paper, we introduce a supersonic spray dryer that enables production of submicron-sized drug substance particles at rates up to 1.5 g/h; this throughput is more than five times higher than that of commercially available spray dryers that produce submicron particles of comparable size.^{26–28} We demonstrate that the particle size of a model API, danazol, can be conveniently tuned between 200 nm and 1.2 μm by adjusting the air pressure at the inlets. By comparison to unprocessed powder danazol, which is commonly used to formulate drug products, the surface to volume ratio of 700 nm diameter particles produced with the spray dryer is increased by a factor of 11; this results in a dissolution rate that is increased by up to four times. By contrast to more traditional spray dryers, only room temperature air is used with our nozzle introduced here, thereby avoiding heating of the drug which can be deleterious to its stability. This new spray-dryer nozzle can be the basis of a new class of spray dryers that produces sub-micrometer particles.

EXPERIMENTAL SECTION

The spray dryer consists of two identical epoxy chips, which are patterned to control the flow of the air when the chips are glued together to form the device. A tapered glass capillary is used to inject the liquid, and two syringe tips are used to inject the dispersing gas as shown in Figure 1a. The syringe tips are connected to 10 cm long polyethylene tubing with an inner diameter of 1.2 mm. This tubing transitions into a 4 mm inner diameter polyethylene tubing, which is connected to dry air pressurized at 690 kPa. We regulate the applied pressure using a valve and measure it with an inline air pressure gauge in the larger tubing. We design the three-dimensional (3D) geometry of the spray dryer with a computer aided design (CAD) software (AutoCad 2015, Autodesk, CA, USA); the spray dryer design is shown in Figure S1a. The initial mold for the chip is printed with an Objet 30 (Stratasys Ltd., Edina, MN, USA), Figure S1b. This is used as a template from which an inverse master is molded using polydimethylsiloxane (PDMS), as shown in Figure S1c. After the PDMS was cured at 65 °C for 2 h, the surface is rendered fluorophilic by immersing it into HFE 7100 (methoxyperfluorobutane, Sigma-Aldrich, USA) containing 0.5 vol/vol % trichloro(1H,1H,2H,2H-perfluorooctyl)silane (Sigma-Aldrich, USA) for 5 min. The inverse master is filled with PDMS to produce the final flexible casting mold, as shown in Figure S1d. The two halves of the spray dryer are cast from the same flexible master using epoxy (EpoxAcast 690 purchased from Smooth-on Inc., Macungie, PA, USA). The epoxy is semicured at 60 °C for 2 h. The key to the operation of the device is the nozzle for the liquid dispersion; it consists of a glass capillary, with a 1 mm outer diameter, that is tapered by a micropipette puller (model P-97, Sutter Instruments, Novato, CA, USA) and is manually sanded to attain an inner nozzle diameter of 80 μm . The glass-capillary is attached to one of the spray dryer blocks, and its position relative to the narrowest cross-section is adjusted manually using a light microscope. The spray dryer is closed with the second semicured epoxy block. The epoxy glue is fully cured for another 2 h at 60 °C, which also enables the two sides to be fully sealed. CAD models of the spray dryer are shown in Figure

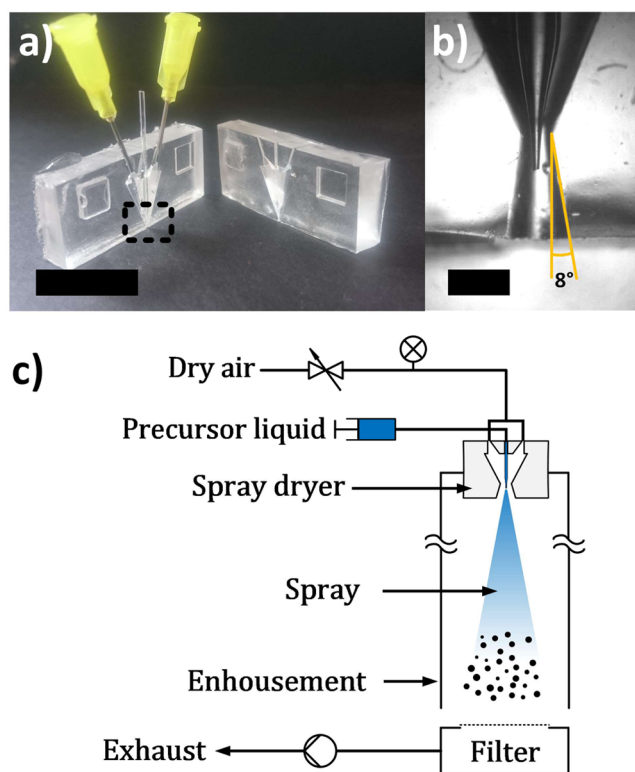


Figure 1. (a) The spray dryer is assembled from two semicured, epoxy-casted parts that encompass a glass capillary for injection of the fluid and two syringe tips for injection of pressurized, dry air. The scale bar is 2 mm. (b) Light microscope image of the de Laval nozzle for supersonic air acceleration. The scale bar is 1 mm. (c) Danazol solution is delivered by a volume driven pump through a glass capillary into a de Laval type nozzle and dispersed by pressurized dry air, forming a fine spray. Dried particles are collected on glass fiber filters using a vacuum pump.

S2. The spray dryer geometry resembles a de Laval type²⁹ nozzle with cone-shaped convergent and divergent parts, joined at the throat, which is a circular, 0.5 mm diameter cross-section as shown in the magnified image in Figure 1b. The inlet diameter of the convergent portion is 10 mm, and the height is 11.3 mm, as shown in Figure S2b. The half-opening angle of the expanding portion is set to 8°, as shown in Figure 1b. This opening angle is chosen to ensure a smooth expansion of the air flow and avoid the formation of a viscous boundary layer and detachment of the flow.^{30,31} The length of the expander varies from 0 to 3 mm, resulting in exit cross-sectional areas between 0.196 mm² and 1.417 mm². The glass capillary is coaxially embedded in the de Laval nozzle and the capillary exit lies inside the divergent nozzle. The setup is schematically shown in Figure 1c. We inject the drug solution into the glass capillary at flow-rates between 100 mL/h and 300 mL/h using stepper-motor-controlled syringe pumps (Harvard Apparatus, Holliston, MA, USA). A vacuum pump (Vacuubrand MZ 2C NT, Essex, CT, USA) connected to the backside of the filter paper (Whatman, grade GF/A, VWR, USA) is used to improve particle collection. The spray dryer is enclosed inside a cardboard box set up in a ventilated hood, to avoid particle exposure during experiments.

The majority of experiments are performed using danazol (BASF SE, Germany) as a model API. Solutions are prepared by dissolving the API in ethanol (200 proof anhydrous Koptec USP, VWR, USA) at concentrations of 1–10 mg/mL. Number-based size distributions of the spray-dried particles are analyzed from scanning electron microscopy (SEM) images (FESEM Supra55VP, Zeiss, 2 keV) using ImageJ software (ImageJ, U.S. National Institutes of Health, Bethesda, MD, USA). Samples for the particle size analysis are prepared by direct particle deposition onto a silicon wafer substrate and are subsequently

sputter coated with 2 ± 0.1 nm of Pt:Pd (20:80 w/w%, MS 300T D Dual Head Sputter Coater, Electron Microscopy Sciences, Hatfield, Pennsylvania, USA) for SEM imaging. Particle size distributions are described by calculating the Sauter mean diameter (SMD):

$$d_{\text{SMD}} = \frac{\sum_{i=1}^n d_i^3}{\sum_{i=1}^n d_i^2} \quad (1)$$

where d_i denotes the diameter of particle i and n denotes the total number of particles analyzed and is always at least 100 particles. The SMD is inversely proportional to the specific surface area and is therefore a critical measure for surface area dependent processes, such as dissolution of particles. The width of the particle size distribution is characterized with the span:

$$\text{span} = \frac{d_{90} - d_{10}}{d_{50}} \quad (2)$$

where d_x is the diameter with $x\%$ of cumulative distribution.

Powder X-ray diffraction (PXRD) measurements are conducted on a Bruker D2 Phaser powder diffractometer (Bruker Corp., Billerica, MA) at $2\Theta = 4-40^\circ$, increment $=0.01^\circ$ and time step $= 0.1$ s. The specific surface area (SSA) of powder samples is measured by nitrogen adsorption using the Brunauer–Emmett–Teller (BET) method (Monosorb, Quantachrome, USA).

Dissolution studies are performed by dissolving known quantities (50 ± 1 mg) of spray-dried danazol particles in 900 mL of dissolution medium, consisting of 2-propanol mixed with 0.1 M hydrochloric acid (4:6 vol/vol %).³² It is constantly stirred with a paddle mixer at 100 rpm. The pH of the dissolution medium is set to 1.20 and maintained at a temperature of 37°C .³³ For these measurements, the concentration of the fully dissolved API dosage must be at least three times lower than the solubility to avoid saturation effects on the dissolution kinetics.³⁴ For the dosages used, the maximum concentration of danazol is 0.055 mg/mL, more than 10 times below that of the saturation concentration, 0.912 mg/mL; this corresponds to sink conditions.³² The API powder is hand filled into hard gelatin capsules size 0 (Wonder Laboratories, White House, TN, USA) and exposed to the dissolution media using a stainless steel cage, to prevent floating of the capsule. The dissolved amount of API is quantified photometrically at 285 nm (Cary 100 UV–Vis spectrophotometer, Agilent Technologies) by analysis of 3 mL samples of the media, retrieved at 5, 10, 15, 20, 30, 45, 60, and 90 min. Prior to dissolution studies, a calibration of danazol in the dissolution medium is carried out. This is achieved by measuring the absorbance of three samples with danazol concentrations of 0.01, 0.02, and 0.04 mg/mL and using a linear fit of the absorbance as a function of concentration for these data as a calibration standard. For comparison, similar measurements are performed on unprocessed powder of danazol.

RESULTS AND DISCUSSION

To enhance the bioavailability of poorly water-soluble drug substances, we aim to generate the smallest possible drug particles by spray drying for which we need the smallest possible droplets. Conventional two-fluid nozzle spray dryers generate droplets by impinging a high velocity gas onto a solution jet. The maximum flow velocity, v , at the converging nozzle exit is limited to the local sonic speed, a , thus limiting droplet size. Supersonic gas flows with shocks could potentially overcome this velocity, and hence, droplet-size limit and fully nebulize the solution jet. In this paper, we use a well-known nozzle design to achieve supersonic flows: a de Laval type nozzle consisting of a converging and diverging portion.²⁹ The dispersing gas accelerates in the converging nozzle, while the cross sectional area is reduced leading to a concomitant reduction in the pressure, density, and temperature. Intuitively, this can be best captured for incompressible flows with a constant density: to conserve mass, the gas has to flow faster

through a smaller cross sectional area than through a larger one to achieve the same throughput. For subsonic flows the gas velocity is maximum in the smallest cross-section of the nozzle, the throat. Gas flows with a Mach number, $Ma = v/a$, smaller 0.3 are well approximated as incompressible. However, as the velocity approaches the speed of sound, compressibility effects become significant and the gas density increases with higher velocity. As the gas flow velocity reaches sonic speed in the throat, the flow is choked. Any further increase of inlet pressure cannot accelerate the throat velocity above sonic speed; it remains at $Ma = 1$ and instead the gas is compressed. The only way to increase the gas velocity above sonic speed is by decreasing the density; this can be achieved by increasing the cross section and expanding the flow. This is accomplished in the de Laval nozzle where the gas relaxes and the pressure decreases in the divergent portion of the nozzle resulting in supersonic flow velocities. The acceleration and deceleration are described by the area-velocity relation of a compressible fluid under isentropic conditions in a pipe,²⁹

$$\frac{dv}{v} = \frac{1}{Ma^2 - 1} \frac{dA}{A} \quad (3)$$

where A is the area. The velocity in a subsonic regime with $Ma < 1$ is increased, $dv > 0$, by decreasing the cross-sectional area, $dA < 0$. By contrast, in a supersonic regime with $Ma > 1$, the fluid is accelerated $dv > 0$ by increasing the cross-sectional area $dA > 0$. The throat is the only position in a converging nozzle to achieve $Ma = 1$. The mass flow rate, \dot{m} , is maximum for choked flow with $Ma = 1$ in the throat.²⁹

$$\dot{m} = \frac{A p_t}{\sqrt{T_t}} \sqrt{\frac{\gamma}{R}} Ma \left(1 + \frac{\gamma - 1}{2} Ma^2 \right)^{-(\gamma+1)/(2(\gamma-1))} \quad (4)$$

where R is the specific gas constant, T_t the total temperature, γ the specific heat ratio, and p_t is the total pressure. Although the flow is choked in the throat with $Ma = 1$ as the inlet or total pressure increases, the mass flow increases linearly:

$$\dot{m} = \underbrace{\frac{A}{\sqrt{T_t}} \sqrt{\frac{\gamma}{R}} \left(1 + \frac{\gamma - 1}{2} \right)^{-(\gamma+1)/(2(\gamma-1))}}_{\text{constant}} p_t \quad (5)$$

We verify the attainment of supersonic conditions by measuring the mass flow as a function of the inlet pressure using only dispersing gas without API solution. The injection of liquid into the nozzle with a low liquid content <1 vol % has no effect on achieving supersonic conditions in the gas flow.^{35,36} Figure S3 shows a linear relation for inlet pressures above approximately 240 kPa confirming the attainment of choked flow in the throat and supersonic conditions in the diverging portion. At least 350 kPa are used in the following experiments for all nozzle designs to ensure supersonic conditions.

Rocket engines are designed to achieve a maximum thrust by operating the nozzle so that the exit pressure, p_e , matches the ambient pressure, p_o , although this is only achieved at one altitude. In contrast to rocket engines, we operate the spray dryer nozzle with lower inlet pressures than the optimal expansion. Thus, we achieve an overexpanded flow with a lower pressure at the nozzle exit than ambient pressure; nevertheless, this flow is sufficient to completely nebulize the droplets. The supersonic flow eventually encounters ambient conditions at the nozzle exit where volume expansion leads to abruptly achieving the ambient density, temperature, pressure, and

velocity at the shock front. This discontinuous process takes place across a very short length scale. The very high velocity and pressure gradients fully nebulize the API solution. We collect the spray-dried particles on Si wafers at 60 cm distance from the expander exit and measure their SMD from SEM images. The particles collected on the Si wafer are dry without any additional heating. Particles sprayed from solutions containing 1 mg/mL danazol with 150 mL/h flow rate, 690 kPa inlet pressure, and a 2 mm expander length have a SMD of 235 nm. This is more than 10 times smaller than particles produced with commercial spray dryers at similar production rates.³⁷ To help elucidate the origin of observed behaviors, we investigate the effect of flow parameters. The particle diameter continuously increases with increasing API concentration as shown in Figure 2a. Particles produced with 10 mg/mL API concentration have a SMD of 772 nm as measured from SEM images or 617 nm determined from BET measurements assuming spheres. This is about three times larger than particles produced with 1 mg/mL, which have a SMD of 235 nm. If each droplet results in one particle after evaporation, the particle diameter, d_p , scales with the initial solute concentration as

$$d_p = d_d \left(\frac{c}{\rho_p} \right)^{1/3} \propto c^{1/3} \quad (6)$$

where d_d is the droplet diameter and ρ_p is the API density of 1200 kg/m³ for danazol.³⁸ The measured particle diameters are in reasonable agreement with our assumption that each droplet forms one particle as shown as the green solid line in Figure 2a. Thus, we can calculate the droplet diameter using the measured particle diameter and API concentration. However, particles produced at solute concentrations above 1 mg/mL are significantly more polydisperse, as shown by the large error bars in Figure 2a. Moreover, sporadic hollow particles with significantly larger diameters are found in SEM images. Hollow particles are recognized as the surface buckles and sometimes even ruptures revealing the outer shell. Hollow particles form during evaporation when the receding surface moves faster than the dissolved API.⁵ Consequently, API is enriched close to the surface, and once supersaturation is reached it can precipitate, forming a shell. The supersaturation concentration at the surface of an evaporating droplet is attained with a larger droplet diameter for increasing danazol concentrations, and so the shells, which are occasionally observed on SEM images, are larger.

The difference between liquid and gas velocity in the nozzle is about 2 orders of magnitude. For example, with an injection rate of 100 mL/h ethanol and an air inlet pressure of 690 kPa, the liquid velocity at the capillary exit, v_l , and the gas velocity at the nozzle exit, v_g , are approximately 6 and 600 m/s, respectively. The gas velocity is calculated for $Ma = 2.8$, which is estimated using the measured mass flow rate as shown in Figure S3 and eq 4 at the nozzle exit.²⁹ We inject 100–300 mL/h of 1 mg/mL danazol/ethanol into a device with a 2 mm long expander to vary the liquid velocity between 6 and 17 m/s. Regardless of the tested injection rates, the particles produced by applying 690 kPa to the air inlets have a diameter of around 200 nm as shown in Figure 2b. A 3-fold increase in the liquid flow rate does not significantly change the difference in relative velocities and, as expected, the particle diameters are independent of the fluid injection rate for the investigated conditions. In contrast, increasing the gas inlet pressure results

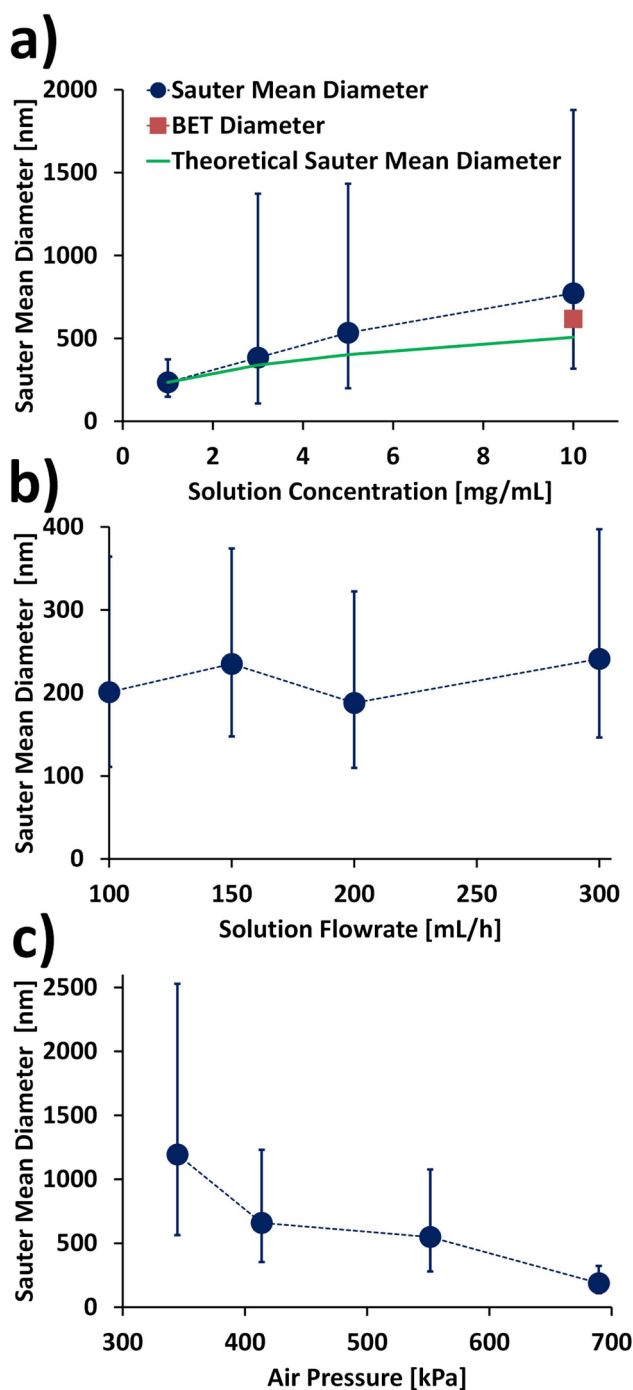


Figure 2. Sauter mean diameter (blue circles) of danazol particles as a function of (a) danazol solution concentration, (b) flow rate, and (c) dispersion air pressure. If each droplet forms one particle, the particle diameter scales with the concentration as shown as a green line in (a). The particle diameter (red square) measured by the Brunauer–Emmett–Teller method is shown in (a) for comparison to the diameter obtained by SEM images. The error bars correspond to one geometric standard deviation.

in a decrease in particle size as shown in Figure 2c. More specifically, increasing the pressure from 345 to 690 kPa results in a reduction of API particle size from 1200 to 200 nm, though the maximum velocity and Mach number at the nozzle exit remain nearly constant. To account for the origin of the effect of process parameters on particle sizes, we consider possible breakup mechanisms of droplets in the spray dryer.

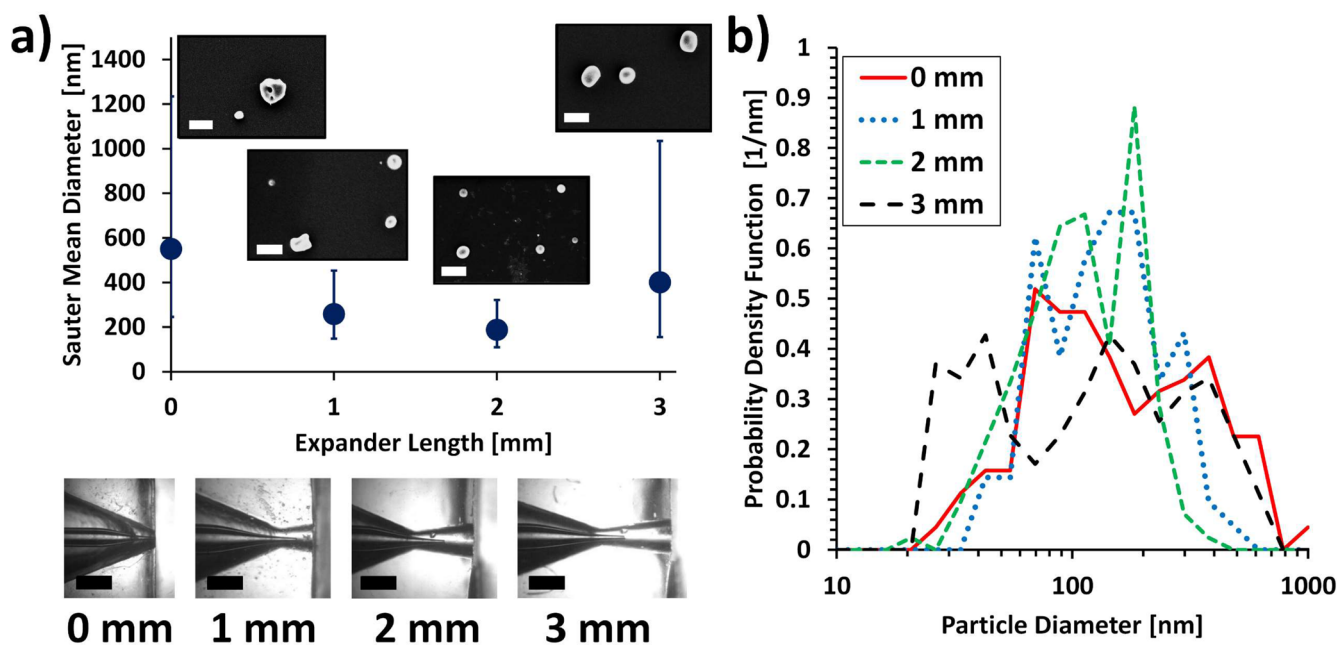


Figure 3. (a) The Sauter mean particle diameter (blue circles) as a function of expander length. Light microscopy images show the four devices with increasing expander length. The smallest particles are produced in spray dryers with 2 mm long expanders. Scanning electron microscope images of spray-dried particles are shown as insets. The scale bars denote 500 nm. The error bars represent the geometric standard deviation of the particle size distribution. (b) The size distributions of particles produced with expander lengths varying from 0 to 3 mm.

Using a concentration of 1 mg/mL danazol 200 nm spherical dense particles are produced from droplets of 2 μm . Several forces can break the injected liquid jet into such fine droplets: for example, the viscous shear stress of the supersonic gas stream can destabilize the liquid jet surface which is held together by surface tension, $\frac{\eta_g(v_g - v_l)}{r_l} = \frac{4\sigma}{d_d}$, where $v_g - v_l$ is the relative velocity between dispersing gas and API solution, r_l is the length scale over which the two velocities adjust, here, the radius of the liquid jet and d_d the droplet size for which the shear and surface tension forces are in equilibrium. Under these conditions, droplets of about 300 μm should form by viscous shear stresses; this is 2 orders of magnitude larger than that estimated from collected API particles. This indicates that viscous shearing is not the dominant mechanism of droplet formation in the present supersonic spray dryer.

Alternatively, the jet can break by Kelvin–Helmholtz instabilities at the liquid–gas interface which forms waves that are sheared-off by the high relative velocity. This results in the formation of droplets of $\sim 1 \mu\text{m}$ in diameter as calculated with the wave breakup model.³⁹ Once droplets are formed, they experience an aerodynamic resistance per cross sectional area of the supersonic flow that can deform them and finally lead to droplet breakage if it is larger than the droplet surface tension, $\frac{1}{2}c_w\rho_g(v_g - v_l)^2 = \frac{4\sigma}{d_d}$, where ρ_g is the gas density and c_w is the drag coefficient of around 0.47 for a smooth sphere at high Reynolds numbers.⁴⁰ The estimated droplet diameter $d_d = \frac{8\sigma}{c_w\rho_g(v_g - v_l)^2}$ is again about 1 μm for the conditions used in the spray dryer. Both droplet breakup mechanisms, the Kelvin–Helmholtz instability and breakup by aerodynamic resistance, predict droplet sizes in the same order of magnitude as that estimated using the measured particle size. However, both breakup mechanisms predict a constant droplet size for increasing inlet pressures as the velocity remains constant,

which conflicts with the experimental results of Figure 2c showing that the particle size decreases. Instead, we hypothesize that the final droplet size is determined by the shock. The pressure drop across the shock as well as the shape and number of shock fronts change with increasing inlet pressure according to the isentropic equations.²⁹ A higher inlet pressure results in a higher pressure drop across the shock fronts and the nozzle produces finer droplets. By extrapolating the data of Figure 2c, we would expect these values to decrease even more if we increased the pressure above 690 kPa while maintaining an overexpanded flow as indicated by above results. However, 690 kPa is the limit of the pressurized air source employed. Even at such high pressures, the device did not show any signs of defects or debonding, indicating that it could sustain even higher pressures; hence, this device could likely produce even smaller particles.

To further support our hypothesis that the shock breaks the droplets, we change the expander length to vary the available distance of air flow acceleration before the shock. A longer expander results in a higher maximum velocity in the nozzle and larger velocity and pressure gradients over the shock.⁴¹ However, the expander cannot be chosen arbitrarily long; the velocity close to the wall is subsonic due to a viscous boundary layer. If the nozzle is too long, the boundary layer thickness increases because of viscous forces and detaches from the wall preventing the acceleration to supersonic flow. We vary the expander length from 0 to 3 mm for a constant inlet pressure of 690 kPa and inject 1 mg/mL danazol in ethanol solution at 200 mL/h. The particle diameter decreases with increasing expander length and reaches a minimum for ~ 2 mm before increasing again as presented in Figure 3a. By increasing the expander length from 0 mm to 2 mm, the particle SMD changes from 551 to 188 nm. The particles produced with a spray dryer having 1 or 2 mm expander length exhibit a narrower size distribution with spans of 1.7 and 1.4, respectively, compared to those produced with 0 or 3 mm

expanders having spans of 2.8 and 3, respectively, as shown in Figure 3b and summarized in Table S2.

To investigate the effect of expander length on the gas velocity and shock front, we simulate the air flow using computational fluid dynamics (CFD). The maximum air velocity in the expander increases with expander length from 501 m/s for devices with no expander to 626 m/s for 2 mm long expanders, as shown in Figure S4a. In addition, CFD simulations reveal pronounced shock fronts right outside of the nozzle exit in the case of 1 mm and 2 mm expanders with pressures at the nozzle exit below ambient pressure, an overexpanded flow, Figure S4b.⁴² In contrast, the 0 mm expander exhibits underexpanded flow with air pressure at the nozzle exit above ambient. No pronounced shock front develops for devices with no expander resulting in lower velocity and pressure gradients than for overexpanded flows. Consistent with this, solid particles with a broad size distribution having a span of 2.8 are formed, as shown in Figure 3b. Unexpectedly, a similarly broad distribution with a span of 3 is obtained if the expander length is increased to 3 mm; the pressure decreases continuously in the diverging part with a shock formed around the capillary exit rather than the nozzle exit as shown in Figure S4a. Danazol solution droplets in devices with 3 mm expanders experience weaker velocity- and pressure-gradients as they do not pass a shock forming larger and more polydisperse particles. These results suggest that the smallest particles with the narrowest size distributions are formed by pronounced shock fronts close to the nozzle exit in overexpanded flows. To demonstrate the versatility of the spray-dryer, we spray sodium chloride particles with a diameter of 566 nm and carbamazepine with 737 nm at production rates above 1 g/h each.

We design our spray dryer to achieve the smallest possible particle size with the highest possible throughput to enhance the dissolution kinetics of poorly water-soluble drugs. We generate danazol particles with diameters of 772 nm at a production rate of 1500 mg/h using a spray dryer with a 2 mm expander length to compare to unprocessed danazol with sizes typically used to formulate drug products. The unprocessed danazol comprises coarse, several micrometer-sized crystals with some fines distributed on their surface. In contrast, the spray-dried particles collected on a filter form a loosely agglomerated film with no obvious distinction between coarse and fine particles. Representative SEM images of the unprocessed and spray-dried powders are shown in Figure 4, panels a and b, respectively, with a magnification of the submicron particles in Figure 4c. The specific surface area of the spray-dried danazol with $8.10 \text{ m}^2/\text{g}$ is more than 11 times higher than that of unprocessed danazol. We evaluate the performance of our submicron spray-dried danazol particles in comparison to the unprocessed particles by measuring the time until 90% of powder is dissolved in 2-propanol mixed with 0.1 M hydrochloric acid (4:6 vol/vol %). We quantify the dissolution kinetics of danazol using UV–vis spectroscopy. Our spray-dried danazol powder dissolves more than four times faster than unprocessed powder as shown in Figure 4d. In addition, the spray-dried powder exhibits a lower variation in dissolution kinetics than the unprocessed powder, which is desirable as it improves predictability. Spray drying can result in amorphous particles due to high drying rates inherent to the process.⁴³ The dissolution rate of drug substances heavily depends on their structure; it is much higher for amorphous particles than for crystalline ones.^{44,45} However, the amorphous

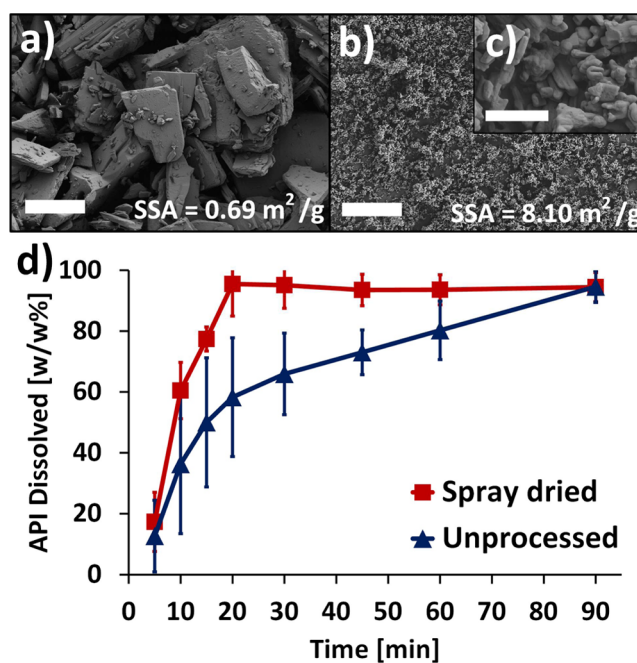


Figure 4. Scanning electron microscopy images of (a) unprocessed and (b) spray-dried danazol with the specific surface area measured by the Brunauer–Emmett–Teller method. The scale bar represents 20 μm . (c) A magnification of the spray-dried powder shows the submicron particle size. The scale bar represents 1 μm . Consistent with these results, the SSA is an order of magnitude higher for the spray-dried particles. (d) Photometrically conducted dissolution studies of unprocessed and spray-dried danazol. The dissolution of the spray-dried powder is significantly faster than that of the unprocessed powder. The error bars correspond to the maximum and minimum amount of dissolved API at each time.

phase is metastable and amorphous particles tend to crystallize over time, for example, during storage.⁴⁶ This results in an uncontrolled change in dissolution kinetics, which prevents the wide application of amorphous API particles for drug formulation without using additives. We characterize the structure of our spray-dried nanoparticles and unprocessed danazol using PXRD. The PXRD pattern of the unprocessed sample matches the pattern of CSD code YAPZEU of preferentially oriented crystals with normal (001). We observe clear diffraction peaks for spray-dried danazol particles. Indeed, the PXRD pattern of spray-dried nanoparticles also closely resembles the pattern calculated with CSD code YAPZEU, as shown in Figure 5, indicating that spray-dried particles are crystalline and potentially stable over time. Furthermore, this confirms that the enhancement in dissolution kinetics is caused by a reduction in particle size rather than the formation of amorphous particles.

CONCLUSIONS AND OUTLOOK

Fully crystalline submicron danazol particles with a particle Sauter mean diameter of 772 nm are produced at a rate up to 1500 mg/h using a novel supersonic spray-dryer. The submicrometer-sized spray-dried danazol particles dissolve more than four times faster than unprocessed danazol powder due to their reduction in particle size. These particles are formed from small droplets that are generated with a supersonic nozzle using shock fronts. Moreover, the drops are sufficiently small and the air flow sufficiently fast that the drops dry so fast at room temperature that the use of heated air, commonly employed to

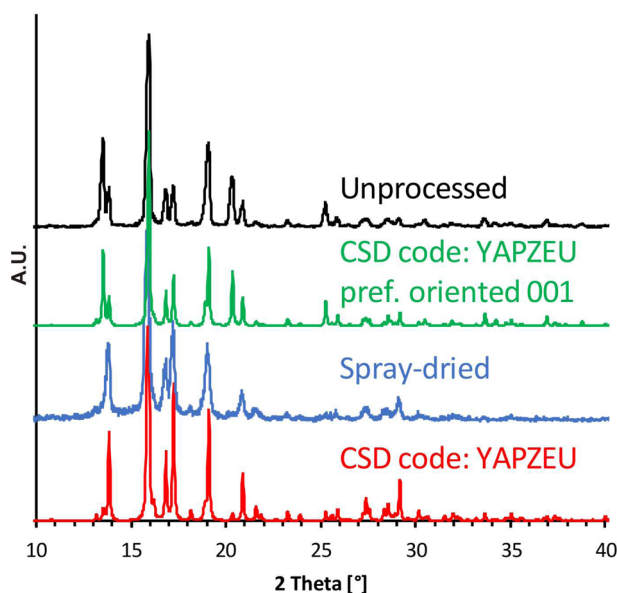


Figure 5. Powder X-ray diffraction patterns show a crystalline structure of danazol after spray drying consistent with Cambridge Structural Database (CSD) code YAPZEU. The unprocessed sample is preferentially oriented with normal (001).

accelerate the drying process, is superfluous. Hence, this device also enables processing of thermolabile substances including biologicals like enzymes that could not be spray-dried using heated air. As the device is based on 3D printed parts and a glass capillary, it could be easily parallelized. Indeed, parallel operation of 10 spray-dryer nozzles would result in a production rate up to 15 g/h or a production of 120 g of API particles in an 8-h day. The presented supersonic spray dryer nozzle has the potential to enable the rapid production of submicron crystalline API particles for drug development.

■ ASSOCIATED CONTENT

Supporting Information

The Supporting Information is available free of charge on the ACS Publications website at DOI: 10.1021/acs.cgd.7b00033.

Figure S1 presents the steps for the production of the spray drying nozzle. Figure S2 shows CAD drawings of the nozzle. Validation of attainment of supersonic flow is shown in Figure S3. Table S1 summarizes the material properties for the CFD simulations. Figure S4 shows CFD results for different expander lengths. Table S2 summarizes the size distributions with varying expander length (PDF)

■ AUTHOR INFORMATION

Corresponding Author

*E-mail: weitz@seas.harvard.edu.

ORCID

David A. Weitz: 0000-0001-6678-5208

Present Addresses

^{||}Novartis Pharma AG, Novartis Campus, P.O. Box, CH-4002 Basel, Switzerland.

[⊥]ABB Switzerland, Brown Boveri Street 6, 5400 Baden, Switzerland.

Author Contributions

[#]M.L.E. and V.K. contributed equally to this work.

Notes

The authors declare no competing financial interest.

■ ACKNOWLEDGMENTS

M.L.E. received funding from the Swiss National Science Foundation (Grant No. P2EZP2-148643). This work was performed in part at the Center for Nanoscale Systems (CNS), a member of the National Nanotechnology Infrastructure Network (NNIN), which is supported by the National Science Foundation under NSF Award No. ECS-0335765. The CNS is part of Harvard University. This work was supported partially by the MRSEC program of the National Science Foundation under Award Number DMR-1420570. We acknowledge the support of James Weaver of the Wyss Institute, Harvard University, for assistance with 3D printing. We thank Ulrich Meier, Andreas Kordikowski, and Aniko Udvarhelyi, all Novartis Pharma AG, and Sebastian Koltzenburg, BASF SE, for productive discussions.

■ REFERENCES

- (1) WHO; WHO Expert Committee on Specifications for Pharmaceutical Preparations, 2015; Vol. 992.
- (2) Ku, M. S.; Dulin, W. *Pharm. Dev. Technol.* **2012**, *17*, 285–302.
- (3) Takagi, T.; Ramachandran, C.; Bermejo, M.; Yamashita, S.; Yu, L. X.; Amidon, G. L. *Mol. Pharmaceutics* **2006**, *3*, 631–643.
- (4) Miller, J. M.; Beig, A.; Carr, R. A.; Spence, J. K.; Dahan, A. *Mol. Pharmaceutics* **2012**, *9*, 2009–2016.
- (5) Vehring, R. *Pharm. Res.* **2008**, *25*, 999–1022.
- (6) Serajuddin, A. T. M. *Adv. Drug Delivery Rev.* **2007**, *59*, 603–616.
- (7) Vyas, A.; Saraf, S.; Saraf, S. J. *Inclusion Phenom. Mol. Recognit. Chem.* **2008**, *62*, 23–42.
- (8) Tiago, J. M.; Padrela, L.; Rodrigues, M. A.; Matos, H. A.; Almeida, A. J.; De Azevedo, E. G. *Cryst. Growth Des.* **2013**, *13*, 4940–4947.
- (9) Pouton, C. W. *Eur. J. Pharm. Sci.* **2006**, *29*, 278–287.
- (10) Lipinski, C. A. *J. Pharmacol. Toxicol. Methods* **2000**, *44*, 235–249.
- (11) Blagden, N.; de Matas, M.; Gavan, P. T.; York, P. *Adv. Drug Delivery Rev.* **2007**, *59*, 617–630.
- (12) Chen, H.; Khemtong, C.; Yang, X.; Chang, X.; Gao, J. *Drug Discovery Today* **2011**, *16*, 354–360.
- (13) Noyes, A. A.; Whitney, W. R. *J. Am. Chem. Soc.* **1897**, *19*, 930–934.
- (14) Merisko-Liversidge, E.; Liversidge, G. G.; Cooper, E. R. *Eur. J. Pharm. Sci.* **2003**, *18*, 113–120.
- (15) Mosharraf, M.; Nystrom, C. *Int. J. Pharm.* **1995**, *122*, 35–47.
- (16) Fisher, E. S. *Encycl. Pharm. Technol.* **2006**, *4*, 2339–2351.
- (17) Matteucci, M. E.; Hotze, M. A.; Johnston, K. P.; Williams, R. O., III. *Langmuir* **2006**, *22*, 8951–8959.
- (18) Thiele, J.; Windbergs, M.; Abate, A. R.; Trebbin, M.; Shum, H. C.; Foerster, S.; Weitz, D. A. *Lab Chip* **2011**, *11*, 2362–2368.
- (19) Zhang, J.-Y.; Shen, Z.-G.; Zhong, J.; Hu, T.-T.; Chen, J.-F.; Ma, Z.-Q.; Yun, J. *Int. J. Pharm.* **2006**, *323*, 153–160.
- (20) Wieckhusen, D. *Chimia* **2006**, *60*, 598–604.
- (21) Bilati, U.; Allemann, E.; Doelker, E. *Eur. J. Pharm. Sci.* **2005**, *24*, 67–75.
- (22) Hede, P. D.; Bach, P.; Jensen, A. D. *Chem. Eng. Sci.* **2008**, *63*, 3821–3842.
- (23) Re, M. I. *Drying Technol.* **2006**, *24*, 433–446.
- (24) Amstad, E.; Gopinadhan, M.; Holtze, C.; Osuji, C. O.; Brenner, M. P.; Spaepen, F.; Weitz, D. A. *Science (Washington, DC, U. S.)* **2015**, *349*, 956–960.
- (25) Kesisoglou, F.; Panmai, S.; Wu, Y. *Adv. Drug Delivery Rev.* **2007**, *59*, 631–644.
- (26) Li, F.; Josephson, D. P.; Stein, A. *Angew. Chem., Int. Ed.* **2011**, *50*, 360–388.

- (27) Heng, D.; Lee, S. H.; Ng, W. K.; Tan, R. B. H. *Expert Opin. Drug Delivery* **2011**, *8*, 965–972.
- (28) Baba, K.; Nishida, K. *Pharmaceutics* **2013**, *5*, 107–114.
- (29) Balachandran, P. *Fundamentals of Compressible Fluid Dynamics*; Prentice-Hall of India Pvt. Ltd: New Dehli, 2006.
- (30) Darbandi, M.; Roohi, E. *Microfluid. Nanofluid.* **2011**, *10*, 321–335.
- (31) Xu, J.; Zhao, C. *Int. J. Heat Mass Transfer* **2007**, *50*, 2434–2438.
- (32) Brown, S.; Rowley, G.; Pearson, J. T. *Int. J. Pharm.* **1998**, *165*, 227–237.
- (33) Vertzoni, M.; Dressman, J.; Butler, J.; Hempenstall, J.; Reppas, C. *Eur. J. Pharm. Biopharm.* **2005**, *60*, 413–417.
- (34) Phillips, D. J.; Pygall, S. R.; Cooper, V. B.; Mann, J. C. *J. Pharm. Pharmacol.* **2012**, *64*, 1549–1559.
- (35) Messerschmidt, R. Dissertation, University of Bonn, 2004.
- (36) Liu, H. *Science and Engineering of Droplets: Fundamentals and Applications*; Elsevier Science: Amsterdam, 2000.
- (37) Park, J.; Park, H. J.; Cho, W.; Cha, K.-H.; Kang, Y.-S.; Hwang, S.-J. *Int. J. Pharm.* **2010**, *396*, 239–245.
- (38) Chempider, <http://www.chemspider.com/>
- (39) Reitz, R. D. *At. Spray Technol.* **1987**, *3*, 309–337.
- (40) Lasheras, J. C.; Hopfinger, E. *Annu. Rev. Fluid Mech.* **2000**, *32*, 275–308.
- (41) Louisos, W. F.; Hitt, D. L. In *Encyclopedia of Microfluidics and Nanofluidics*; Springer: Berlin, 2014; pp 1–18.
- (42) Lee, M. W.; Park, J. J.; Kim, D. Y.; Yoon, S. S.; Kim, H. Y.; Kim, D. H.; James, S. C.; Chandra, S.; Coyle, T.; Ryu, J. H.; Yoon, W. H.; Park, D. S. *J. Aerosol Sci.* **2011**, *42*, 771–780.
- (43) Vehring, R.; Foss, W. R.; Lechuga-Ballesteros, D. *J. Aerosol Sci.* **2007**, *38*, 728–746.
- (44) Laitinen, R.; Lobmann, K.; Strachan, C. J.; Grohgan, H.; Rades, T. *Int. J. Pharm.* **2013**, *453*, 65–79.
- (45) Babu, N. J.; Nangia, A. *Cryst. Growth Des.* **2011**, *11*, 2662–2679.
- (46) Ng, Y. C.; Yang, Z.; McAuley, W. J.; Qi, S. *Eur. J. Pharm. Biopharm.* **2013**, *84*, 555–565.